Analysis of the Beaucage model
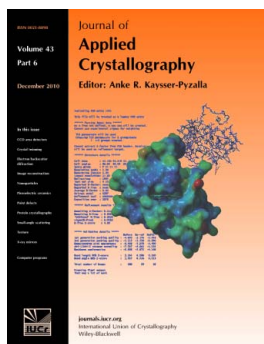
Boualem Hammouda

Many research topics in condensed matter research, materials science and the life sciences make use of crystallographic methods to study crystalline and non-crystalline matter with neutrons, X-rays and electrons. Articles published in the *Journal of Applied Crystallography* focus on these methods and their use in identifying structural and diffusion-controlled phase transformations, structure–property relationships, structural changes of defects, interfaces and surfaces, *etc.* Developments of instrumentation and crystallographic apparatus, theory and interpretation, numerical analysis and other related subjects are also covered. The journal is the primary place where crystallographic computer program information is published.

Crystallography Journals Online is available from **journals.iucr.org**

Analysis of the Beaucage model

Boualem Hammouda

National Institute of Standards and Technology, Center for Neutron Research, 100 Bureau Drive, Gaithersburg, MD 20899, USA. Correspondence e-mail: hammouda@nist.gov

The Beaucage model is used to analyze small-angle scattering (SAS) data from fractal and particulate systems. It models the Guinier and Porod regions with a smooth transition between them and yields a radius of gyration and a Porod exponent. This model is an approximate form of an earlier polymer fractal model that has been generalized to cover a wider scope. The practice of allowing both the Guinier and the Porod scale factors to vary independently during nonlinear least-squares fits introduces undesired artefacts in the fitting of SAS data to this model. Such artefacts as well as an error in the original formulation of the model are discussed. This model is compared with other published models.

1. Introduction

Small-angle scattering (SAS) is a popular characterization technique at the nanometre length scale. SAS data analysis consists of standard linear plots (such as the Guinier and Porod plots) as well as nonlinear least-squares fits to models. The Guinier plot yields a radius of gyration that characterizes the size of the scattering particles, while the Porod plot yields an exponent that suggests a substructural dimensionality from which the overall particle shape can be guessed. Porod exponents between 1 and 3 describe mass fractals, while exponents between 3 and 4 indicate surface fractals. A number of books have been published in the field (Guinier & Fournet, 1955; Glatter & Kratky, 1982; Feigin & Svergun, 1987; Roe, 2000; Lindner & Zemb, 2002). Many models are available to describe various molecular architectures. These include polymer coils and particles of many shapes. Models that describe non-particulate systems that are characterized by bicontinuous (or multiphase) structures are also available (Teubner & Strey, 1987; Chen & Choi, 1997). Uniform density particles are used to describe multiphase systems, globular scattering objects, microdomains, colloids, precipitates and so on.

The Guinier model consists in a linear plot of $\log[I(Q)]$ versus Q^2, where Q is the scattering variable and $I(Q)$ is the scattered intensity for compact objects. The slope is $R_g^2/3$, where R_g is the radius of gyration of the scattering objects. A generalized Guinier plot (Glatter & Kratky, 1982) is used to obtain the radii of gyration for nonspherical particles such as cylinders or platelets. For cylinders, a plot of $\log[QI(Q)]$ versus Q^2 gives a slope of $R_g^2/2$, where R_g is the cross-sectional radius of gyration ($R_g = R/2^{1/2}$, where R is the cylinder radius) at intermediate Q. The low-Q Guinier plot remains of the form $\log[I(Q)]$ versus Q^2, with R_g representing the overall size $[R_g = (L^2/12 + R^2/2)^{1/2}$, where L is the cylinder length]. For square platelets, there are also two Guinier regions. One is at intermediate Q, for which the Guinier plot changes to $\log[Q^2 I(Q)]$ versus Q^2. The slope is $R_g^2/1$, with $R_g = T/12^{1/2}$ given in terms of the platelet thickness T. The other Guinier region, at low Q, is the standard $\log[I(Q)]$ versus Q^2 plot, which yields $R_g = (L^2/6 + T^2/12)^{1/2}$, where L is the platelet length. Particles with three orthogonal sizes are characterized by three Guinier regions. The lowest-Q Guinier region is always the standard one and yields the overall particle radius of gyration.

The Porod plot consists of a linear plot of $\log[I(Q)]$ versus $\log(Q)$. The slope is the Porod exponent (also referred to as power law). This exponent points to either mass fractals (Teixeira, 1988) or surface fractals (Bale & Schmidt, 1984). Fractals are self-similar structures that appear analogous at different length scales. A quick Porod plot of reduced SAS data gives clues as to the nature of the scattering structures. Some structures display multiple Porod regions at the various size scales. For example, a $1/Q^2$ behavior at low Q may point to platelets (for example, crystalline lamellae) or to a network of rigid rods, while the same $1/Q^2$ behavior at high Q could point to Gaussian polymer coils.

The SAS scattering intensity is proportional to a single particle (or single polymer) form factor and to an interparticle structure factor. Form factors have been modeled for particles of different shapes. Elongated shapes require an orientational averaging integration. Modeling of structure factors is more involved. Interparticle structure factors are usually described by the Ornstein–Zernike equation in its various closure forms, while homogeneously mixed polymers are described by the random-phase approximation. Empirical models help analyze SAS data without involved modeling effort.

The Beaucage model was introduced some 15 years ago and was presented as an empirical model to fit SAS data and obtain a radius of gyration and a Porod exponent. This model has been used widely in the SAS community. A literature search using the advanced search feature of the Google search engine and the keywords 'Beaucage model' resulted in over 250 hits. This model is critically analyzed in the present paper

and compared with other molecular models as well as with a recent empirical model called the Guinier–Porod model.

2. The polymer fractal model

A model describing polymer chain conformations with excluded volume has been used as a template for describing mass fractals. The form factor for this model (Benoit, 1957) was originally presented in the following integral form:

$$P(Q) = 2 \int_0^1 dx(1 - x) \exp\left[-(Q^2 a^2/6)n^{2\nu}x^{2\nu}\right]. \quad (1)$$

Here ν is the excluded volume parameter, which is related to the Porod exponent d as $\nu = 1/d$, a is the polymer chain statistical segment length, n is the degree of polymerization and x is the integration variable. This integral was later put into an analytical form (Hammouda, 1993) as follows:

$$P(Q) = \frac{1}{\nu U^{1/2\nu}} \gamma\left(\frac{1}{2\nu}, U\right) - \frac{1}{\nu U^{1/\nu}} \gamma\left(\frac{1}{\nu}, U\right). \quad (2)$$

Here, $\gamma(x, U)$ is the incomplete gamma function, which is a built-in function in computer libraries:

$$\gamma(x, U) = \int_0^U dt \exp(-t)t^{x-1}. \quad (3)$$

The variable U is given in terms of the scattering variable Q as

$$U = Q^2 a^2 n^{2\nu}/6 = Q^2 R_g^2 (2\nu + 1)(2\nu + 2)/6. \quad (4)$$

The radius of gyration squared has been defined as

$$R_g^2 = \frac{a^2 n^{2\nu}}{(2\nu + 1)(2\nu + 2)}. \quad (5)$$

Note that this model describing polymer chains with excluded volume applies only in the mass fractal range ($5/3 \leq d \leq 3$) and does not apply to surface fractals ($3 < d \leq 4$). It does not reproduce the rigid-rod limit ($d = 1$) because it assumes chain flexibility from the outset, nor does it describe semi-flexible chains ($1 < d < 5/3$).

The low-Q expansion yields the Guinier form and the high-Q expansion yields the Porod form, which is given by

$$P(Q \to \infty) = \frac{1}{\nu U^{1/2\nu}} \Gamma\left(\frac{1}{2\nu}\right) - \frac{1}{\nu U^{1/\nu}} \Gamma\left(\frac{1}{\nu}\right). \quad (6)$$

Here $\Gamma(x) = \gamma(x, \infty)$ is the gamma function. The asymptotic limit is dominated by the first term:

$$\begin{aligned} P(Q \to \infty) &\simeq \frac{d}{U^{d/2}} \Gamma\left(\frac{d}{2}\right) \\ &= \frac{d}{(QR_g)^d}\left[\frac{6d^2}{(2+d)(2+2d)}\right]^{d/2} \Gamma\left(\frac{d}{2}\right). \quad (7) \end{aligned}$$

The special case when $\nu = 0.5$ (or $d = 1/\nu = 2$) corresponds to Gaussian chains for which the form factor is given by the familiar Debye function:

$$P(Q) = \frac{2}{Q^4 R_g^4}\left[\exp(-Q^2 R_g^2) - 1 + Q^2 R_g^2\right]. \quad (8)$$

The form factor given by equation (2) is plotted in Fig. 1 for specific Porod exponents d.

3. The Beaucage model

Beaucage introduced a model based on the polymer fractal model. He used the numerical integration form (Benoit, 1957), although the analytical integral form was available (Hammouda, 1993). The Beaucage (1995, 1996) model is characterized by three fitting parameters: a Guinier scaling factor G, a radius of gyration R_g and a Porod exponent d. The scattering intensity is given by

$$I(Q) = G \exp\left(\frac{-Q^2 R_g^2}{3}\right) + \frac{C}{Q^d}\left[\text{erf}\left(\frac{QR_g}{6^{1/2}}\right)\right]^{3d}. \quad (9)$$

Since the Guinier form applies at low Q and the Porod form applies at high Q, the $[\text{erf}(QR_g/6^{1/2})]^{3d}$ term provides a smooth transition between the two regions.

The Porod scaling factor C is related to the Guinier scaling factor G using the high-Q expansion of the polymer fractal model as follows:

$$C = \frac{Gd}{R_g^d}\left[\frac{6d^2}{(2+d)(2+2d)}\right]^{d/2} \Gamma\left(\frac{d}{2}\right). \quad (10)$$

The original form [equation (8) given by Beaucage (1996)] was in error; it was missing the factor $\{6d^2/[(2+d)(2+2d)]\}^{d/2}$ and therefore is correct for Gaussian chains only ($d = 2$). Here $\Gamma(d/2)$ is the gamma function. This form comes from the high-Q expansion of the polymer fractal model [equation (7) above].
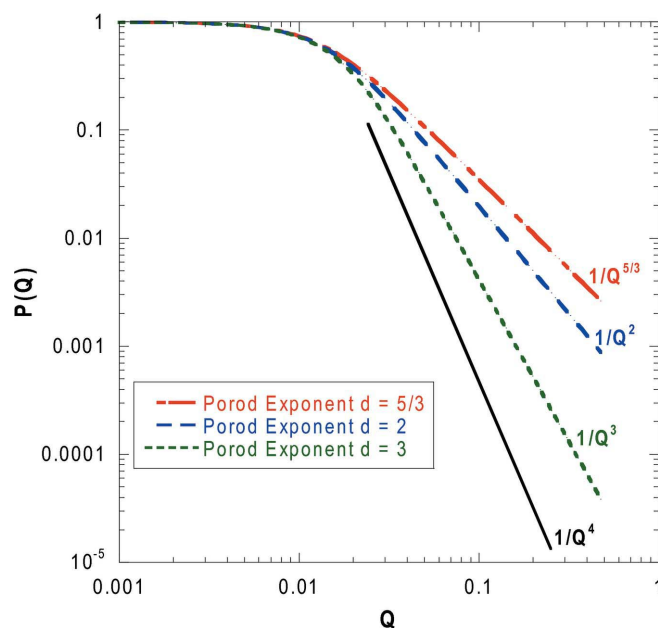

Figure 1
The polymer fractal model for $R_g = 100$ Å and for various Porod exponents: $d = 5/3$ for fully swollen chains, $d = 2$ for ideal Gaussian chains and $d = 3$ for collapsed chains. The $1/Q^4$ Porod law limit is also shown, although it does not apply to the polymer fractal model.

Fig. 2 shows the various terms of the Beaucage model.

In order to correct for the mismatch between the Guinier and Porod scale factors caused by the aforementioned error, a fudge factor k was introduced (Beaucage, 1996). This fudge factor works only partially since it is trying to correct for a 'vertical' mismatch through a 'horizontal' rescaling.

The corrected Beaucage model is a good approximation to the exact polymer fractal model, as shown in Fig. 3. Fig. 3 compares these two models as well as the original form of the Beaucage model with equation (10) missing the square
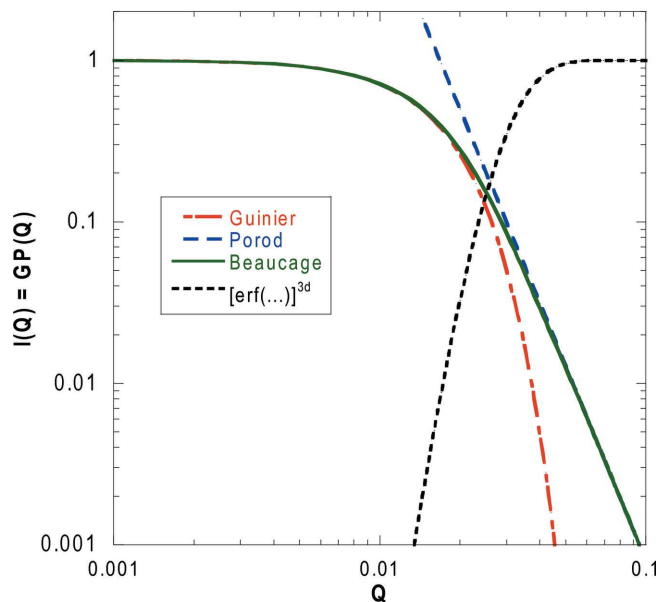

Figure 2
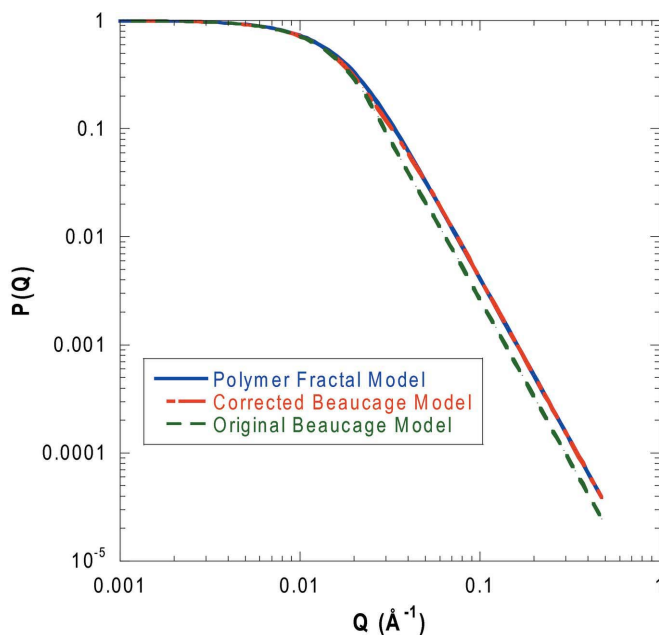The various terms for the Beaucage model for $G = 1$, $R_g = 100$ Å and $d = 3$.

Figure 3
Comparison of the corrected Beaucage model [equations (9) and (10)] and the polymer fractal model [equation (2)] for $G = 1$, $R_g = 100$ Å and $d = 3$. These two fall on top of each other. The original Beaucage model with the square bracket term in equation (10) missing is also included.

bracket factor. Note that the Beaucage model is presented as an empirical model even though, originally, it was obtained from the polymer fractal model. After the correction to match equation (10), the Beaucage model and the polymer fractal model agree well without any need for a fudge factor. The small difference in the transition region between the two models is due to the $[\mathrm{erf}(QR_g/6^{1/2})]^{3d}$ term used to provide a smooth transition.

Letting the Porod scale factor C vary independently yields an erroneous artefact that shows up as a kink (break in the slope) in the Porod region. This artefact is obvious in papers using the Beaucage model in the literature as well as in papers by Beaucage. For instance, Figs. 11–14 in one of the original papers (Beaucage, 1995) show the artefact clearly, as does Fig. 4(b) from a more recent paper (Beaucage & Kulkarni, 2010). In order to demonstrate this artefact, parameters from Fig. 12 of the original paper (Beaucage, 1995) are used here to plot Fig. 4. These parameters are $G = 100$, $R_g = 87.9$ and $d = 4.91$. Three curves are plotted with various choices for the Porod scale factor. Curve (a) uses $C = 1.9 \times 10^{-8}$ (value used in the legend of Fig. 12), curve (b) uses $C = 1.804 \times 10^{-7}$ [value corresponding to equation (10) above with the square bracket term missing] and curve (c) uses $C = 7.338 \times 10^{-7}$ [value corresponding to the full equation (10) above]. All of these curves show the artefact except for the one using the full equation (10) of this paper.

4. The Guinier–Porod model

An empirical Guinier–Porod model was recently introduced (Hammouda, 2010). The scattering intensity is given by the two contributions
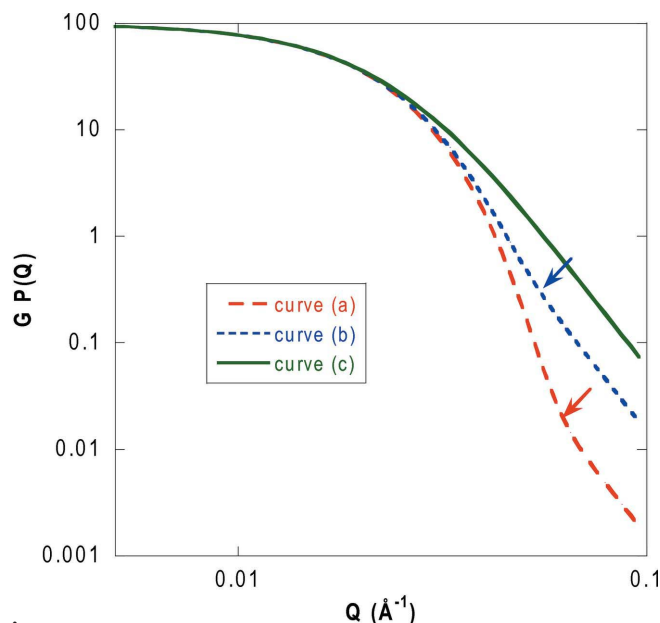

Figure 4
The artefact caused by letting both the Guinier and the Porod scale factors vary independently is seen in curves (a) and (b). Curve (c), which corresponds to equation (10) of this paper, is the only curve without the artefact. Arrows point to the break in slope.

Table 1
Comparing fits to the Beaucage and the Guinier–Porod models for 0.5% P85/d-water at a temperature (T) of 303 and 323 K.

The 303 K case corresponds to a mass fractal (copolymers in solution), while the 323 K case corresponds to well formed spherical micelles.

T (K)	Model	G	R_g (Å)	d	Q range (Å^{-1})
303	Beaucage	0.287 (3)	53.51 (79)	1.65 (2)	0.0107–0.385
303	Guinier–Porod	0.279 (3)	45.41 (49)	1.30 (1)	0.0107–0.385
323	Beaucage	7.67 (1)	47.09 (5)	8.39 (99)	0.0038–0.075
323	Guinier–Porod	7.55 (1)	46.03 (9)	3.97 (9)	0.0038–0.075

$$I(Q) = G \exp\left(-Q^2 R_g^2/3\right) \quad \text{for} \quad Q \leq Q_1,$$
$$I(Q) = D/Q^d \quad \text{for} \quad Q \geq Q_1. \tag{11}$$

Imposing the condition that the values of the Guinier and Porod terms and their slopes (derivatives) be continuous at a value Q_1 yields the following relationships:

$$Q_1 = \frac{1}{R_g}\left(\frac{3d}{2}\right)^{1/2},$$
$$D = G \exp\left(\frac{-Q_1^2 R_g^2}{3}\right) Q_1^d = G \exp\left(-\frac{d}{2}\right)\left(\frac{3d}{2}\right)^{d/2} \frac{1}{R_g^d}. \tag{12}$$

It should be emphasized that, in order to connect up the two (Guinier and Porod) functions, two conditions are required. This ensures smoothness in the horizontal as well as in the vertical directions at the transition region.

In order to compare the performance of the Beaucage and the Guinier–Porod models, nonlinear least-squares fits were performed for small-angle neutron scattering data from 0.5% Pluronic P85 in deuterated water (d-water) at 303 K, representing copolymer coils in solution, and at 323 K, where spherical micelles are formed (Hammouda, 2010). Table 1 compares the results.

Both the Guinier–Porod and the Beaucage models yield reasonable results for the 0.5% P85/d-water at 303 K. This corresponds to a polymer mass fractal. For the 323 K case where well formed spherical micelles are present, the Guinier–Porod model yields the expected Porod exponent for spherical micelles, while the corrected Beaucage model yields values of the Porod exponent that are too high. The polymer fractal model and its approximate form, the Beaucage model, work best for Porod exponents in the range $5/3 \leq d \leq 3$. They do not do well for Porod exponents higher than 3, such as for spherical micelles.

5. Comparison of various models

The Beaucage model and the Guinier–Porod model are compared with various known form factor models. The polymer fractal model and its approximate form, the Beaucage model, are characterized by

$$\frac{CR_g^d}{G} = d\left[\frac{6d^2}{(2+d)(2+2d)}\right]^{d/2} \Gamma\left(\frac{d}{2}\right). \tag{13}$$

The Guinier–Porod model is characterized by

Table 2
Comparison of the ratios CR_g^d/G (Beaucage model) and DR_g^d/G (Guinier–Porod model) with known values obtained from exact form factor calculations.

Model	$d = 1$	$d = 2$	$d = 3$	$d = 4$
Beaucage model	1.253	2	4.170	10.24
Guinier–Porod model	0.743	1.104	2.130	4.872
Thin rigid rod	0.895	–	–	–
Gaussian coil	–	2	–	–
Thin disc	–	1	–	–
Uniform density sphere	–	–	–	1.62
Randomly oriented cylinder with $R = L$	–	–	–	1.94

$$\frac{DR_g^d}{G} = \exp\left(-\frac{d}{2}\right)\left(\frac{3d}{2}\right)^{d/2}. \tag{14}$$

These are compared in Table 2 for discreet values of d. Known values of these ratios obtained from the high-Q expansions of the following form factors are also included:

(*a*) Thin rigid rod of uniform density and length L (case with $d = 1$):

$$P(Q) = \frac{2}{QL}\sin(QL) - \left[\frac{\sin(QL/2)}{(QL/2)}\right]^2 \overset{QL \gg 1}{\longrightarrow} \frac{3.1}{QL} = \frac{0.895}{QR_g}. \tag{15}$$

The radius of gyration for a thin rod of length L ($R_g = L/12^{1/2}$) has been used.

(*b*) Gaussian coil (case with $d = 2$):

$$P(Q) = \frac{2}{Q^4 R_g^4}\left[\exp(-Q^2 R_g^2) - 1 + Q^2 R_g^2\right] \overset{QR_g \gg 1}{\longrightarrow} \frac{2}{(QR_g)^2}. \tag{16}$$

(*c*) Thin disc of radius R (also case with $d = 2$):

$$P(Q) = \frac{2}{(QR)^2}\left[1 - \frac{J_1(2QR)}{QR}\right] \overset{QR \gg 1}{\longrightarrow} \frac{2}{(QR)^2} = \frac{1}{(QR_g)^2}. \tag{17}$$

$J_1(2QR)$ is the cylindrical Bessel function, and the radius of gyration for a thin disc of radius R ($R_g = R/2^{1/2}$) has been used.

(*d*) Uniform density sphere of radius R (case with $d = 4$):

$$P(Q) = \left[\frac{3j_1(QR)}{QR}\right]^2 \overset{QR \gg 1}{\longrightarrow} \frac{9}{2}\frac{1}{(QR)^4} = \frac{1.62}{(QR_g)^4}. \tag{18}$$

$j_1(QR)$ is the spherical Bessel function, and the radius of gyration of a sphere of radius R [$R_g = (3/5)^{1/2}R$] has been used.

(*e*) Randomly oriented cylinder of radius R and length L (case with $d = 4$). The case where $R = L$ is considered for simplicity in order to estimate the high-Q asymptotic limit:

$$P(Q) = \frac{1}{2}\int_{-1}^{1} d\mu \left[\frac{\sin(Q\mu L/2)}{Q\mu L/2}\right]^2 \left\{\frac{2J_1[Q(1-\mu^2)^{1/2}R]}{Q(1-\mu^2)^{1/2}R}\right\}^2$$
$$\overset{QL \gg 1}{\longrightarrow} \frac{5.7}{(QL)^4} = \frac{1.94}{(QR_g)^4}. \tag{19}$$

The radius of gyration of a cylinder of length L and radius $R = L$ $[R_g = (7/12)^{1/2}R]$ has been used.

The polymer fractal model and its approximate form (the Beaucage model) perform perfectly well for the Gaussian coil case ($d = 2$), while the Guinier–Porod model is closer to the known exact values for the rigid rod, the disc, the uniform sphere and the randomly oriented cylinder cases. Neither model performs well for the last two cases (surface fractals).

6. Summary

The Beaucage model has been widely used to analyze SAS data. It is the approximate form of an exact polymer fractal model. For this reason, it works best for mass fractals characterized by Porod exponents between 5/3 and 3. This model was upgraded to an empirical model status whereby both the Guinier and the Porod scale factors are allowed to vary independently. The Guinier and Porod functions must be linked both horizontally and vertically in the transition region. The horizontal linking is performed using an error function transition. By letting both the Guinier and the Porod scale factors vary independently, the vertical linking was relaxed. This creates undesired artefacts that show up as kinks in the fitted curve.

The original idea of the Beaucage model could be useful in modeling form factors that involve numerical integrations (over random orientations, for example). This would speed up the model function numerical calculations during nonlinear least-squares fits. The Guinier and Porod scale factors, however, must be related by the correct form obtained from the exact calculation of the form factor. A few of these forms are included in Table 2 for specific particle shapes.

References

Bale, H. D. & Schmidt, P. W. (1984). *Phys. Rev. Lett.* **53**, 596–599.
Beaucage, G. (1995). *J. Appl. Cryst.* **28**, 717–728.
Beaucage, G. (1996). *J. Appl. Cryst.* **29**, 134–146.
Beaucage, G. & Kulkarni, A. (2010). *Macromolecules*, **43**, 532–537.
Benoit, H. (1957). *C. R. Hebd. Seances Acad. Sci.* **245**, 2244–2247.
Chen, S.-H. & Choi, S.-M. (1997). *J. Appl. Cryst.* **30**, 755–760.
Feigin, L. A. & Svergun, D. I. (1987). *Structure Analysis by Small-Angle X-ray and Neutron Scattering.* New York: Plenum Press.
Glatter, O. & Kratky, O. (1982). *Small-Angle X-ray Scattering*, London: Academic Press.
Guinier, A. & Fournet, G. (1955). *Small-Angle Scattering of X-rays.* New York: John Wiley and Sons.
Hammouda, B. (1993). *Adv. Polym. Sci.* **106**, 87–133.
Hammouda, B. (2010). *J. Appl. Cryst.* **43**, 716–719.
Lindner, P. & Zemb, T. (2002). *Neutrons, X-rays and Light: Scattering Methods Applied to Soft Condensed Matter.* Amsterdam: Elsevier.
Roe, R. J. (2000). *Methods of X-ray and Neutron Scattering in Polymer Science.* New York: Oxford University Press.
Teixeira, J. (1988). *J. Appl. Cryst.* **21**, 781–785.
Teubner, M. & Strey, R. (1987). *J. Chem. Phys.* **87**, 3195–3200.